INFLUENCE OF CONTACT INTERFACE DESIGN OVER THE BOND FORMATION OF 3D PRINTED PARTS

Ermolai, Vasile [a1,b]; Sover, Alexandru [a2]; and Nagîţ, Gheorghe [b]

[a] Ansbach University of Applied Sciences, Faculty of Technology, Residenzstraße 8, 91522 Ansbach. Germany. ([a1] vasile.ermolai@hs-ansbach.de, [a2] a.sover@hs-ansbach.de)
[b] "Gheorghe Asachi" Technical University of Iasi, Department of Machine Manufacturing Technology, Blvd. D. Mangeron, 59A, 700050 Iasi. Romania. (nagit@tcm.tuiasi.ro)

ABSTRACT: Fused Filament Fabrication (FFF) is an additive manufacturing technology that uses molten thermoplastic materials forced through a nozzle to build parts layer-wise and enables the manufacturing single and multiple materials parts. The multi-material interface bond strength influences the resulting part integrity. The interface represents the physical boundary between materials, and its shape depends on the part's design. However, the most common interface designs are based on a flat surface-to-surface contact. Thus, this paper aimed to investigate if the interface strength of polylactic acid-based (PLA) parts can be enhanced by designing new interface geometries with a sinusoidal and zig-zag pattern orientated in two directions. The resulting interfaces were tested mechanically and analyzed under the microscope to describe bond formation. The results show that interface shape orientation and overlap between mating bodies significantly influence the multi-material interface strength.

KEY WORDS: 3D Printing, Fused Filament Fabrication, Multi-material interface, Interfacial bonding, Bond strength.

1. INTRODUCTION

Fused Filament Fabrication (FFF) is an extrusion-based additive manufacturing technology in which parts are built by selectively depositing a thermoplastic material (Gibson et al., 2021; Hasanov et al., 2021). To be deposited and maintain their extruded shape, the polymeric materials are heated and extruded in a viscous state in the form of filaments (Gibson et al., 2021) (often known as lines (Ghostkeeper, 2023)).

The extruded lines are deposited on the previous or next to the adjacent lines creating intimate contact and developing interfaces. This contact between the deposited material and the other filaments is known as coalescence (Charlon et al., 2021; Lepoivere et al., 2021; Benarbia et al., 2023) and is influenced by the material rheological properties and the pressure exercised by the nozzle. As the material cools, the polymeric chains diffuse, creating molecular bonds and entanglements with the other filaments. This adhesion mechanism between the filaments characterizes the overall strength of the resulting parts (Watschke, 2018; Benarbia et al., 2023).

FFF enables the manufacturing of multi-material parts in a single printing process by using equipment capable of swapping the filaments or using one with multiple extrusion systems (Hazrat et al., 2021). The mechanical properties of the multi-material parts are given by the polymer's adhesion at the level of the Multi-Material Interface (MMI), the boundary between the parts. However, their chemical affinity limits molecular diffusion between different polymers (Watschke, 2018; García-Collado et al., 2022; Cunha et al., 2023). The contact interface area is crucial for multi-material parts made of compatible materials, as the MMI strength is obtained through diffusion (Lopes et al., 2019). For this reason, parts with reduced MMI area present low mechanical properties.

Several studies have been done to increase the bond strength between materials at the interface level by designing MMIs capable of increasing the intimate contact area between materials. Ando et al. (2021) studied the effect of inclined interfaces for tensile samples of PLA with side-by-side mating bodies. With an overlap between mating bodies, this solution increases MMI strength by creating vertical and horizontal contact areas. Frenkel et al., 2022 studied the performance of a woven interface to alternate the material layers for the same type of samples made of PETG and TPU. The results show that this MMI solution's strength is superior to the regular interface.

This paper aimed to study the effect of MMI design on mechanical properties and bond formation using different PLA blends. This way, the resulting interfaces were designed based on five parameters with defined values. Then the interfaces were printed as samples to evaluate the tensile and impact properties. Furthermore, the resulting MMIs were analyzed under the microscope to describe the bond formation.

2. METHODS

2.1 Design of experiment

The MMI interface designs were defined using five parameters with two levels of variation and organized based on a half-factorial experimental matrix (2^5). A sinusoidal and zig-zag pattern constrained by pitch (PP) and height (PH) was considered to improve the bond formation at the MMI level by increasing the contact area between layers. The pattern directions were orientated based on two directions, the y, and the z-axis. On the one hand, using the y-axis orientation, the resulting patterns will increase the vertical contact area between layers. On the other hand, the orientation of the pattern on the z-axis increases the area of horizontal contact between the stacked layers. An overlap between

multi-material parts bodies was considered to increase the bond formation between layers and compensate for extrusion inconsistencies (Ermolai et al., 2021). The chosen levels for each of the presented variables are presented in Table 1.

Table 1. Experimental matrix of the half factorial experimental plan (25) and the result obtained at the tensile and Charpy impact test, where σ represents the stress, ε the strain, and acU is the impact strength.

Run	Pattern	Direction	PP. (mm)	PH. (mm)	Ovp. (μm)	Avg. σ (MPa)	Avg. ε (%)	Avg. a_{cU} (kJ/m^2)
R1	sin	y	0.8	04	0	29.57±0.27	3.56±0.15	4.45±0.54
R2	zig-zag	z	1.6	0.4	100	25.07±1.10	2.79±0.17	4.50±0.46
R3	sin	y	0.8	0.6	100	29.81±0.67	3.68±0.14	6.40±0.67
R4	zig-zag	z	1.6	0.6	0	13.50±0.40	1.44±0.05	4.85±0.60
R5	sin	z	0.8	0.4	100	18.67±3.19	1.93±0.38	4.39±0.97
R6	zig-zag	y	1.6	0.4	0	27.12±0.34	3.14±0.05	4.96±0.76
R7	sin	z	0.8	0.6	0	28.65±1.14	3.34±0.21	4.17±1.33
R8	zig-zag	y	1.6	0.6	100	29.53±0.66	3.54±0.14	6.31±0.28
R9	zig-zag	z	0.8	0.4	0	18.96±2.02	2.01±0.22	5.04±0.62
R10	sin	y	1.6	0.4	100	27.44±0.37	3.08±0.06	6.35±0.47
R11	zig-zag	z	0.8	0.6	100	27.95±0.70	3.30±0.17	5.10±0.22
R12	sin	y	1.6	0.6	0	27.27±0.51	3.05±0.08	6.49±0.90
R13	zig-zag	y	0.8	0.4	100	25.08±0.96	3.16±0.16	3.50±0.32
R14	sin	z	1.6	0.4	0	10.29±0.94	1.08±0.09	3.52±1.40
R15	zig-zag	y	0.8	0.6	0	25.90±1.12	3.29±0.09	3.01±0.53
R16	sin	z	1.6	0.6	100	27.76±0.70	3.21±0.11	3.43±0.87
			Regular Interface (RI)			19.28±0.75	1.63±0.08	3.65±0.49w

The resulting interface configurations were printed as samples. For the tensile testing, the MMIs were designed based on specimen 1B of ISO 527-2 (Figure 1) and impact testing based on specimen 1 of ISO 172-1. A preview of the resulting MMIs designed by respecting the variables described in Table 1 is presented below. To better understand how the chosen parameters influence the bond formation, supplementary samples were printed for optical analysis of the MMIs for each configuration of variables in Table 1.
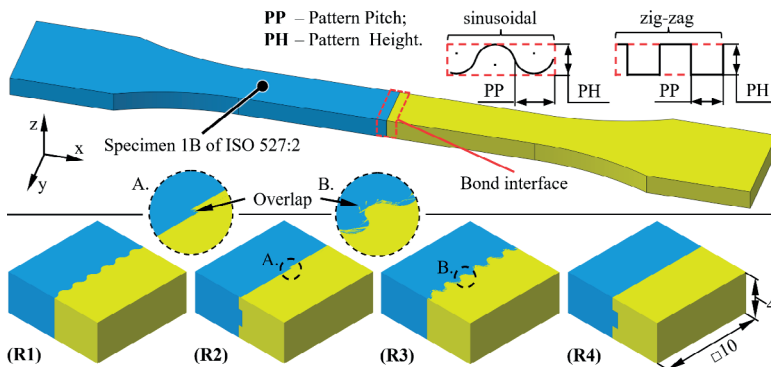

Figure 1. Multi-material interface design of the tensile samples. The resulting interfaces for R1-R4 variables configuration of Table 1.

2.2 Samples' manufacturing and preparation

All samples were printed on a BCN 3D Sigma X R19 using two PLA blends, blue and yellow, manufactured by BCN 3D using the main parameters described in Table 2. Five replicates were printed for each run covered in the experimental plan for the tensile test, ten samples for the Charpy impact test, and two for the optical analysis of the MMIs bond formation.

Wall ordering and *Alternate mesh removal* are two parameters that significantly influence the printing process of the MMIs. If we look at the contact interfaces of the mating bodies described in Figure 1, it can be observed that the external side surfaces of the mating bodies define the MMI. In FFF, the surface of a part is created through a filament (commonly known as a wall or perimeter). The *wall ordering* was set from *Inside to outside* for this experimental setup (Table 2). This way, the inner walls are deposited first (i.e., three walls) and then followed by the outer wall. As the adjacent deposited walls support the molten material, the *Inside to outside* printing sequence could increase material fuse at the MMI level.

Alternate mesh removal is a parameter available in Cura in the *Mesh fixe*s tab. By activating this parameter, the slicer removes a volume of one of the part bodies to make a place for the mating body. This way, a woven structure is created at the MMI level consisting of horizontal and vertical adhesion areas at the level of each layer (Mihalache et al., 2022). The horizontal adhesion area can be further extended by overlapping the part's mating bodies.

Table 2. FFF printing process parameters for BCN Cura 3.2.

	Process parameters	Value		Process parameters	Value
1	Layer thickness (mm)	0.2	13	Printing temperature (°C)	210
2	Extrusion width (mm)	0.4	14	Bed temperature (°C)	60
3	Inner wall extrusion width (mm)	0.38	15	Printing speed (mm/s)	45
4	Number of walls	4	16	First layer printing speed	20
5	Seam alignment on x (mm)	75/-75	17	Print jerk (mm/s)	20
6	Seam alignment on y (mm)	10/-10	18	Outer wall jerk (mm/s)	5
7	Walls ordering	Inside to outside	19	Fan speed (%)	90
			20	Regular fan speed at layer	3
8	Number of top/bottom layers	5	21	Brim width (mm)	6
9	Top/Bottom layers pattern	Lines	22	Purge tower size (mm)	25x25
10	Top/W	40/135	23	Merged meshes overlap (mm)	0
11	Infill pattern	Grid	24	Alternate mesh removal	Active
12	Infill density (%)	50		Italic values are associated with the left-side extruder.	

The samples for optical analysis have a 10x10 mm cross-section and the same thickness of 4 mm as the mechanical trials' samples (Figure 2). Surface preparation consisted of grounding the samples with a Strues Labo Force 100 machine in several steps to obtain a mirror-gloss surface finish. Abrasive papers with grits of 180, 500, 1000, 2000, and

4000 were used. All operations were carried out in the presence of a water jet to avoid warping or melting the workpiece. Finally, the polishing was carried out with a solution of abrasive particles with a diameter of 3 μm. The samples which describe the MMIs' xy plane were ground up to 2 mm, and those for the xz plane up to 5 mm (Figure 3-7).

The mechanical tests were carried out in the same laboratory conditions, in an environment having a temperature of 22°C and 55% humidity. Tensile tests were performed using an Instron 4411 uniaxial testing machine with a load capacity of 5kN. The impact strength was determined using a Zwick 5102.21 Charpy test machine using a 2J pendulum.

The optical analysis was carried out to characterize layers bonding at the interface level. The MMI analysis was performed using a Keyence Vhx 7000 digital microscope.

3. RESULT AND DISCUSSION

3.1 Mechanical strength

Overall, the tensile test results, presented as bar plots in Figure 2, show that compared to the Regular Interface (RI), the newly designed interfaces recorded improved tensile properties in stress and strain.
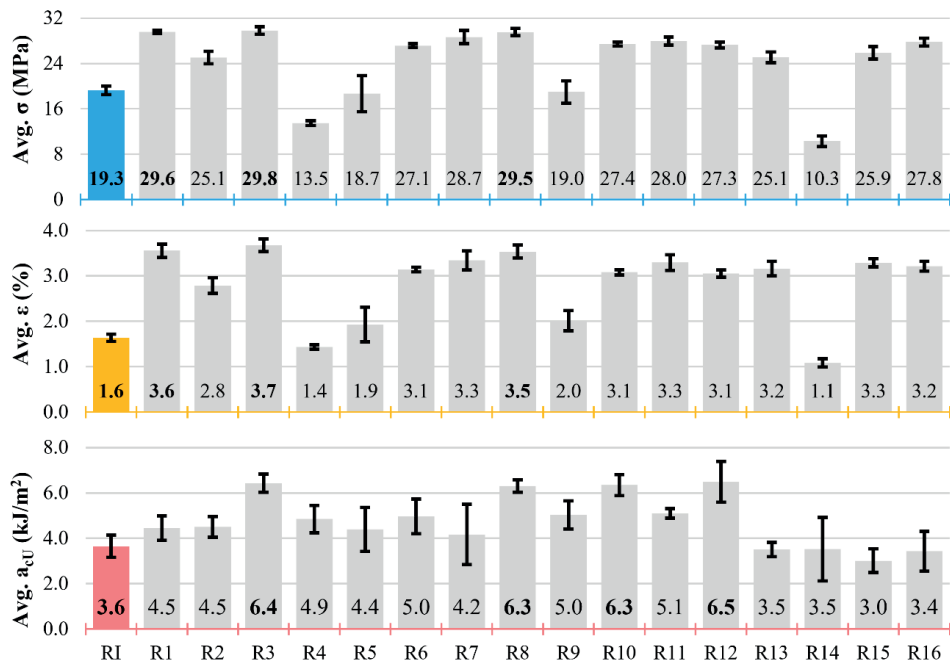

Figure 2. Average stress, strain, and impact strength of the MMI configurations of Table 1 compared to the RI.

From the 16 tested MMI configurations, the best results were obtained by the y-axis orientation of the patterns. The R1, R2, and R3 obtained the highest load capacities, showing an average stress above 29.5 MPa and an average strain above 3.5% (Table 1). Compared to the RI, the R1, R2, and R3 MMI show an increase of ≈53% in stress and ≈118% in strain. Withal, MMI designs such as R4 and R14 recorded stress and stain values lower than RI. These MMIs are characterized by the z-axis orientation of the profile and without overlap between the mating bodies (Table 1).

The Charpy impact test results were obtained for unnotched samples with a flatwise orientation. Overall, samples with a sinusoidal pattern orientated on the y-axis recorded the highest impact energy absorption. R3, R8, and R12 MMI configurations showed an impact strength of over 6.3 kJ/m^2 (see Table 1 and Figure 2). Those results represent an increase of ≈75% in impact energy absorption compared to the RI. The R10 MMI obtained comparable results with a zig-zag pattern on the same y-axis orientation.

3.2 Bonding analysis

Figure 3 shows the structure of a regular multi-material interface. As can be seen, the *Alternate mesh removal* parameter positively influences the formation of vertical and horizontal bonds between materials by creating an alternating deposition.

The front view of the part (Figure 3b) shows an alternating deposition of the two materials at the interface. In the same representation, it can be seen that the degree of alternation is inconsistent both in the top-bottom and left-right directions. At the base layers, the degree of alternation is higher (290-421 μm), and as new layers are deposited, the degree of alternation decreases, reaching a minimum in the middle zone (71-81 μm) and then increases again towards the upper layers (156-180 μm). This pattern was observed for all MMI analyzed.
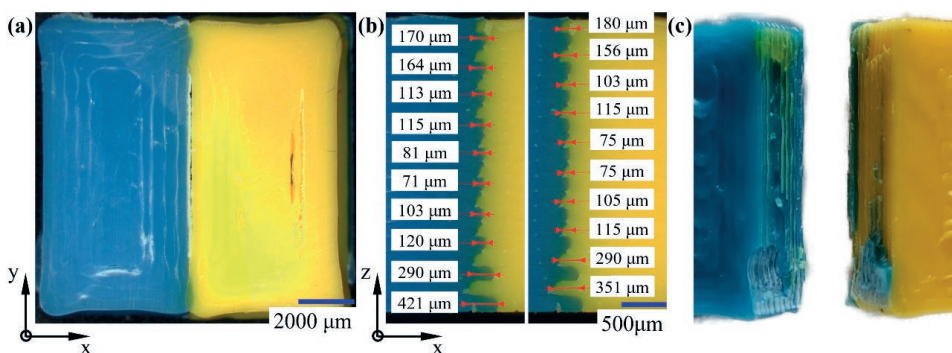

Figure 3. Internal structure of the RI (a) top view; (b) front view; (c) MMI failure mode at tensile test.

In the top view of the same part (Figure 3a), a partial bond of the two materials can be seen on the sample's extremities (green color areas). In the central area of the RI, a void between the materials was observed and can be correlated with the 71-81 μm alternation in the adjacent view (Figure 3b). The identified void in any of the printed samples can explain the poor mechanical properties of the RI (Table 1). From Figure 3c, it can be observed that RI has a poor adhesion of the samples' bodies. The fracture respects the RI profile, and the resulting pieces present traces of the mating material.

Figure 4 shows the internal structure of the R1 MMI (Table 1). The two materials' deposition path follows the interface's sinusoidal shape. Even though the degree of overlap between parts' bodies is zero, both views of the MMI show a smaller variation in alternation between layers. Except for the base layers (first three), which have an alternation of 667-825 μm, the layers show an alternation of 411-492 μm (Figure 4a), increasing slightly for the top layers. From the top view, it can be seen that changing the geometry of the MMI void formation reduced. Instead, a clear bond between materials can be observed (the green color sinusoidal line from Figure 4a). The effect of the improved horizontal bonding can also be seen in the breaking mode of the MMIs (Figure 4c). The fracture respects the pattern's sinusoidal shape but is located on the blue material side.
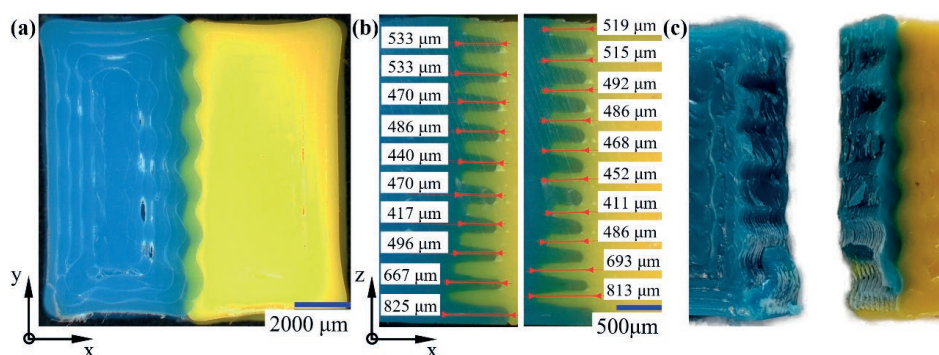

Figure 4. Internal structure of the R1 MMI (a) top view; (b) front view; (c) MMI failure mode at tensile test.

Figure 5 shows the structure of the R2 interface with a zig-zag pattern in the z-direction with 100 μm overlap between the bodies. The alternation between layers shown in the front view maintains the same pattern of variation as previously presented samples. Even though the samples' bodies were printed in superposition, the alternation degree is comparable with the R1 sample (without overlap). On the other hand, comparing the part with a similar zig-zag pattern without overlapping (see Figure 7), we observe that the parts' bodies overlap increases the horizontal contact area between the layers and, therefore, the mechanical properties (Table 1). Even with the increased horizontal contact area, the samples fail at the MMIs level (Figure 5c).
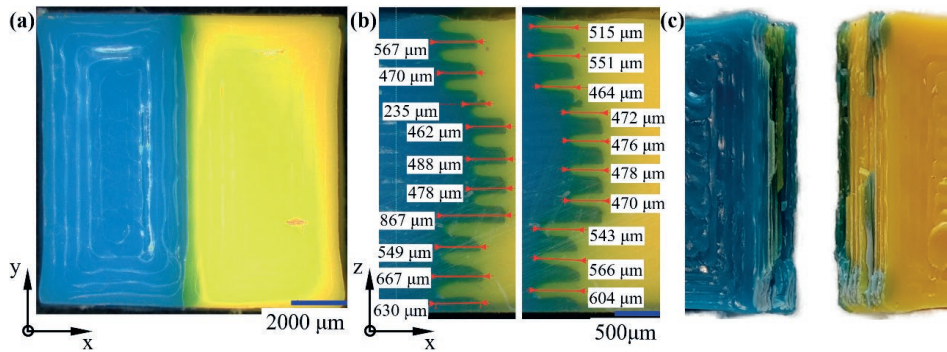
Figure 5. Internal structure of the R2 MMI (a) top view; (b) front view; (c) MMI failure mode at tensile test.

Figure 6 shows an MMI specific to the R3 configuration of parameters, with a sinusoidal profile oriented along the y-axis and a 100 µm overlap between bodies (Table 1). In contrast to the part with the same MMI pattern and direction in Figure 4, the resulting layers alternation is about 100 µm larger (Figure 6b), a value that coincides with the overlap. The increase in the horizontal bond area can be seen in the top view of the MMI (Figure 6a). From a mechanical perspective, the parts with the R3 parameter configuration obtained the best results in the tensile tests (Table 1). Samples failure partially respects the sinusoidal pattern. Due to the increased horizontal contact between layers, the fractures of R3 samples appeared in the body of the blue material at a distance of 1-2 material lines from the midplane (Figure 6c).
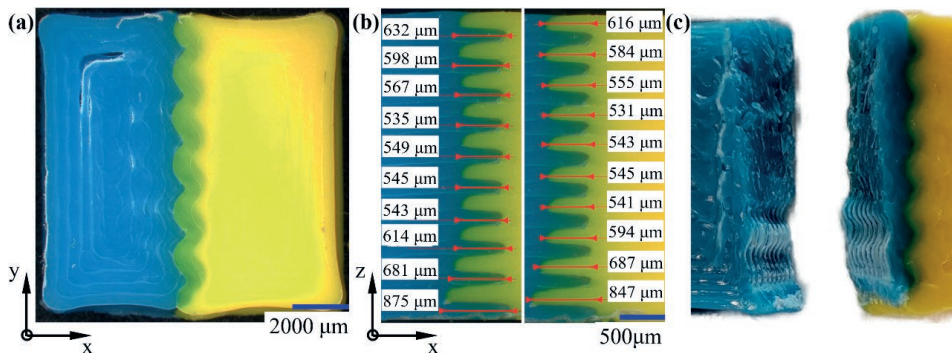

Figure 6. Internal structure of the R3 MMI (a) top view; (b) front view; (c) MMI failure mode at tensile test.

The R4 interface in Figure 7 is described by a zig-zag pattern with vertical orientation and no overlap between parts' bodies. The front view of the part shows that the alternation degree between the materials at the interface level is, on average ≈350 µm (except for

the base layers). This value is ≈100 µm smaller than there resulting horizontal bond areas of the R2 MMIs, with a similar pattern and 100 µm overlap. The small contact area between materials at the interface explains the poor results of the R4 MMI obtained in the mechanical tests (see Table 1 and Figure 2). Regarding the failure of R4 samples, from the example presented in Figure 7c, it can be observed that the absence of the overlap leads to a detachment of the MMIs layers with fewer traces of the mating material compared to R2 samples.
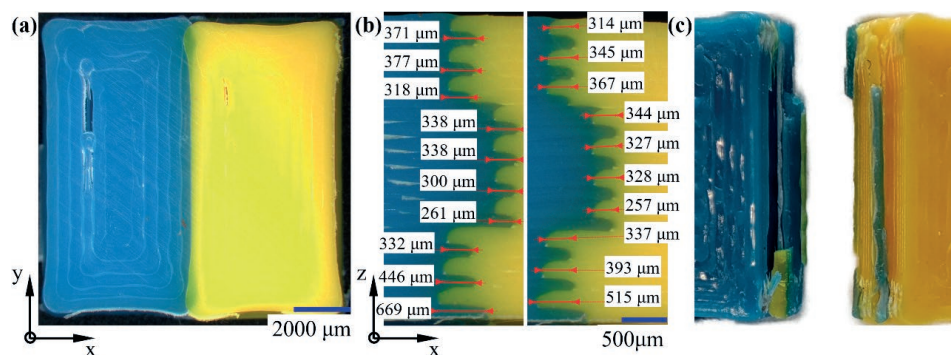

Figure 7. Internal structure of the R4 MMI (a) top view; (b) front view; (c) MMI failure mode at tensile test.

The variable degree of layer alternation at the MMI level can be explained by the filament cooling and solidification and the instantaneous speed of the extrusion systems during deposition.

3.3 Discussion

First, it can be observed that all analyzed MMIs show a higher degree of alternation at the base layers. This effect is caused by the FFF process parameter: *Regular fan speed after layer*, set at 3 (Table 2). This way, the cooling fan will start at the beginning of the fourth layer. During deposition, the first three layers solidify more slowly. Thus, the shrinkage of the material during solidification is smaller. This corresponds to the measured values. In the case of the first layer, the alternation is significantly higher due to the heat released by the build plate at the temperature of 60°C, a value close to the PLA glass transition temperature.

In the case of FFF, the instantaneous speed (often named Jerk (Ghostkeeper, 2023)) at the change of direction is always greater than zero, and its maximum value depends on the equipment. Otherwise, the material, which is constantly fed, overflows and affects the quality of the part. Thus, when changing the direction of travel for the outer wall, the travel speed of the extrusion system decreases to 5 mm/s, then returns to the normal deposition speed of 45 mm/s for the 10 mm width of the MMI, then decreases again

to 5 mm/s, to change the direction of travel again, followed by another return to the initial speed. As the material is in a viscous, semi-liquid state, it can be "pulled" by the printing head and thus deviate from the deposition path. The filaments' shrinkage can amplify this effect during solidification. These assumptions can explain the decrease in the horizontal contact area of R2 and R4 MMIs.

The effects described above are insignificant for parts with the profile arranged along the y-axis. Because the pattern is characterized by frequent direction changes, the print head travels the entire interface at the instantaneous speed of 5 mm/s. This way, the print head movements do not influence the deposition and bonding mechanism.

4. CONCLUSIONS

Multi-material FFF has introduced new possibilities for part manufacturing, allowing for multiple materials in the same components. However, further research is needed in order to improve the strength of the resulting multi-material interfaces.

Modifying the contact interface shape and providing an alternated deposition between the specimen bodies improved the mechanical properties of PLA-printed samples. Compared to the regular but-join interfaces, it was possible to obtain an increase of ≈53% for stress and ≈118% for strain at the tensile tests and an improvement of ≈75% in impact energy absorption for three of the MMIs designs.

The considered interface pattern and orientations help identify that regardless of the considered pattern, orientating it on the y-axis direction is the most beneficial for the strength of the parts. However, the features must be assisted by an overlap between the mating bodies and an alternated deposition at the interface level to increase the horizontal adhesion between layers.

CONFLICT OF INTERESTS

The authors declare no conflict of interest.

AUTHOR CONTRIBUTIONS

E.V. conceived, designed, and performed experiments, analyzed the results, and wrote the manuscript. S.A. and N.G. analyzed the experiments and technical proof of results and reviewed the manuscript. All authors have read and agreed to the published version of the manuscript.

REFERENCES

Andó, M., Birosz, M., & Jeganmohan, S. (2021). Surface bonding of additive manufactured parts from multi-colored PLA Materials. *Measurement*, *169*, 108583. https://doi.org/10.1016/j.measurement.2020.108583

Benarbia, A. (2023). Fused filament fabrication: Numerical adhesion modeling suitable for semicrystalline polymers. *Materials Research Proceedings*, *28*, pp. 139-142. https://doi.org/10.21741/9781644902479-16

Charlon, S., Le Boterff, J., & Soulestin, J. (2021). Fused filament fabrication of polypropylene: Influence of the bead temperature on adhesion and porosity. Additive Manufacturing, *38*, 101838. https://doi.org/10.1016/j.addma.2021.101838

Cunha, P., Teixeira, R., Carneiro, O. S., & Silva, A. F. (2022). Multi-material fused filament fabrication: An expedited methodology to assess the affinity between different materials. *Progress in Additive Manufacturing*, *8(2)*, pp. 195–204. https://doi.org/10.1007/s40964-022-00322-6

Ermolai, V., Sover, A., & Nagîţ, G. (2022). Influence of contact geometry over the filament bond of polylactic acid blends. *IOP Conference Series: Materials Science and Engineering*, *1235(1)*, 012004. https://doi.org/10.1088/1757-899x/1235/1/012004

Frenkel, D., Ginsbury, E., & Sharabi, M. (2022). The mechanics of bioinspired stiff-to-compliant multi-material 3D-printed interfaces. *Biomimetics*, *7(4)*, 170. https://doi.org/10.3390/biomimetics7040170

García-Collado, A., Blanco, J.M., Gupta, M.K., & Dorado-Vicente, R. (2022). Advances in polymers based multi-material additive-manufacturing techniques: State-of-art review on properties and applications. *Additive Manufacturing*, *50*, 102577. https://doi.org/10.1016/j.addma.2021.102577

Gibson, I., Rosen, D., Stucker, B., Khorasani, M., Gibson, I., Rosen, D., & Khorasani, M. (2021). Material extrusion. In: *Additive Manufacturing Technologies*, Springer, Cham. pp. 171-201. https://doi.org/10.1007/978-3-030-56127-7_6

Ghostkeeper (2023, June 10). Ghostkeeper/SettingsGuide: More extensive explanations of cura slicing settings. GitHub. https://github.com/Ghostkeeper/SettingsGuide

Hasanov, S., Alkunte, S., Rajeshirke, M., Gupta, A., Huseynov, O., Fidan, I., Alifui-Segbaya, F., & Rennie, A. (2021). Review on additive manufacturing of multi-material parts: Progress and challenges. *Journal of Manufacturing and Materials Processing*, *6(1)*, 4. https://doi.org/10.3390/jmmp6010004

Hazrat Ali, M., & Abilgaziyev, A. (2021). Fused Deposition Modeling Based 3D Printing: Design, Ideas, Simulations. In Dave, H. K., & Davim, J. P. (Eds.), *Fused Deposition Modeling Based 3D Printing*, pp. 23-42. https://doi.org/10.1007/978-3-030-68024-4_2

Lepoivre, A., Levy, A., Boyard, N., Gaudefroy, V., & Sobotka, V. (2021). Coalescence in fused filament fabrication process: Thermo-dependent characterization of high-performance polymer properties. *Polymer Testing*, *98*, 107096. https://doi.org/10.1016/j.polymertesting.2021.107096

Lopes, L.R., Silva, A.F., & Carneiro, O.S. (2018). Multi-material 3D printing: The Relevance of Materials Affinity on the boundary interface performance. *Additive Manufacturing, 23*, pp. 45–52. https://doi.org/10.1016/j.addma.2018.06.027

Mihalache, A.M., Ermolai, V., Sover, A., Nagîț, G., Boca, M.A., Slătineanu, L., Hrițuc, A., Dodun, O., & Rîpanu, M.I. (2022). Tensile behavior of joints of strip ends made of polymeric materials. *Polymers*, *14*(22), 4990. https://doi.org/10.3390/polym14224990

Watschke, H., Waalkes, L., Schumacher, C., & Vietor, T. (2018). Development of novel test specimens for characterization of multi-material parts manufactured by material extrusion. *Applied Sciences*, *8*(8), 1220. https://doi.org/10.3390/app8081220